Journal of Structural Geology 30 (2008) 1288–1299

Contents lists available at ScienceDirect

Journal of Structural Geology

journal homepage: www.elsevier.com/locate/jsg

# Displacement and interaction of normal fault segments branched at depth: Implications for fault growth and potential earthquake rupture size

R. Soliva [a,*], A. Benedicto [b], R.A. Schultz [c], L. Maerten [d], L. Micarelli [e]

[a] Université Montpellier II, Place E. Bataillon, Laboratoire Géosciences Montpellier – UMR 5243 – Bât. 22 CC 60, 34095 Montpellier Cedex 5, France
[b] Université Paris Sud – Paris XI, Laboratoire de Tectonique – UMR 7072 – Bât. 504, 91405 Orsay Cedex, France
[c] Geomechanics–Rock Fracture Group, Department of Geological Sciences and Engineering/172, Mackay School of Earth Sciences and Engineering, University of Nevada, Reno NV 89557, USA
[d] IGEOSS, Cap Omega, Rond Point Benjamin Franklin, CS39521, 34960 Montpellier Cedex 2, France
[e] BEICIP-FRANLAB, 232 Av. Napoléon Bonaparte, BP 213, 92502 Rueil-Malmaison, France

ARTICLE INFO

*Article history:*
Received 21 April 2008
Received in revised form 11 July 2008
Accepted 14 July 2008
Available online 31 July 2008

*Keywords:*
Fault segmentation
Displacement
Fault interaction
Branching
Earthquake rupture length

ABSTRACT

We present field data from segmented normal faults having particular displacement and overlapping geometries that may be related to down-dip branching of the fault segments. Based on a 3-D numerical modeling study of computed displacement and stress fields around different geometries of down-dip branched normal fault segments, we show that the bends of fault surfaces that coalesce at depth exert a significant influence on (1) the displacement distribution on the fault segment branches and (2) the quasi-static stress fields around the relay zones. The asymmetry in the displacement profiles and low fault interaction at relay zones modeled are consistent with the fault segment geometries observed in field data. As an application, we model the geometry and interaction of the Vallo di Diano normal fault which is segmented at the Earth's surface and which produced an earthquake of magnitude 6.4 along a single fault surface at depth. Numerical modeling of the segmented fault produces an asymmetric displacement profile and low shear stress at the relay zone consistent with the profile and fault interaction inferred from the field. We conclude that asymmetry of the displacement profile and large overlap/separation ratio of the unlinked relay zone can be indicators of the presence of a continuous fault surface underneath. These geometrical attributes are therefore important to consider in the probabilistic analysis of seismic hazard along segmented normal faults.



## 1. Introduction

The three-dimensional (3-D) geometry of faults has been described from high-resolution seismic surveys (e.g. Koledoye et al., 2000, 2003; Kattenhorn and Pollard, 2001; Benedicto et al., 2004) showing that faults are discontinuous and segmented in three dimensions. During their growth, fault segments can propagate from multiple initiation points to form relay ramps and subsequently link to constitute a single coalesced corrugated fault surface (Peacock and Sanderson, 1991; Mansfield and Cartwright, 1996; Crider and Pollard, 1998; McLeod et al., 2000; Gupta and Scholz, 2000; Cowie and Roberts, 2001; Kattenhorn and Pollard, 2001; Marchal et al., 2003). An alternative model of fault segmentation development proposes the bifurcation of a fault into multiple fault segment branches apparent as separated and unlinked on a two-dimensional (2-D) inspection plane (Huggins et al., 1995; Childs et al., 1996; Nicol et al., 1996; Willemse, 1997; Vermilye and Scholz, 1999; Marchal, 1997; Marchal et al., 2003; Walsh et al., 2003a). This style of segmentation is frequently suggested from earthquake rupture of multiple fault segments of length much smaller than the thickness of the seismogenic crust (e.g. Wallace et al., 1984; Philip et al., 1992; Cello et al., 2003; Ferrill et al., 1999). The identification of this fault geometry is therefore of major importance for the prediction of potential earthquake rupture dimensions (Fig. 1). Although the quality of 3-D seismic imagery and seismotectonic studies suggests that subsurface fault segments can be branched at depth, there are no structural or geomorphic criteria that could be used to determine whether fault segments are branched or not which could then provide constraints on potential earthquake rupture size.

High-resolution 3-D seismic surveys demonstrate that two normal fault segments can merge into a single plane at depth along a branch line (Boyer and Elliott, 1982; McGrath and Davison, 1995; Childs et al., 1995; Walsh et al., 1999) or on a branch point (Childs et al., 1995; Marchal et al., 2003). The geometry of overlapping fault segments above a branch line from a seismic survey is shown in

* Corresponding author. Tel.: +33 4 67 14 32 78.
*E-mail address:* roger.soliva@gm.univ-montp2.fr (R. Soliva).

0191-8141/$ – see front matter © 2008 Elsevier Ltd. All rights reserved.
doi:10.1016/j.jsg.2008.07.005

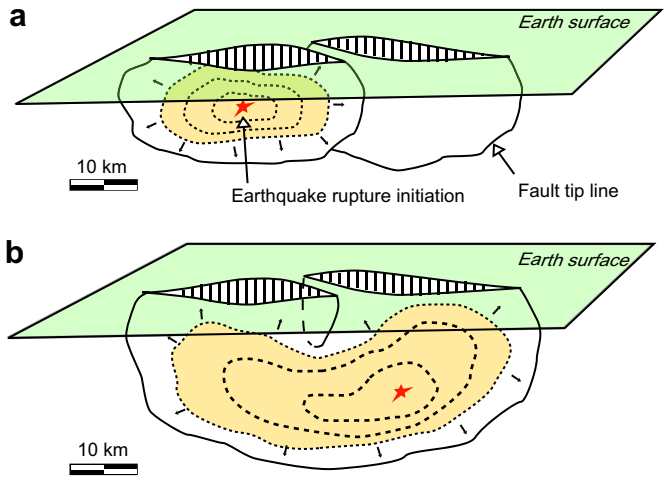


**Fig. 1.** Comparison between (a) separated fault segments and (b) fault segments branched below the Earth's surface (i.e. down-dip branched fault segments). Hypothetical earthquake rupture surface is represented on each case of fault segmentation. Note that the area of the rupture surface in the case of branched fault segments can be twice that for separated fault segments.

Fig. 2, revealing non-homogeneous displacement patterns close to the branch line. In analogy with separated (i.e. non-branched and parallel) interacting normal fault segments, the lateral interaction of down-dip branched segments produces a relay ramp with a high displacement gradient whose segments link as fault displacement accumulates (Childs et al., 1995; Huggins et al., 1995; Marchal et al., 2003; Soliva and Benedicto, 2004). Linkage occurs as fault segments overlap during their strong fault interaction through their stress fields (e.g. Crider and Pollard, 1998; Mansfield and Cartwright, 2001; Young et al., 2001). This stage has been documented as a function of a critical *displacement/segment spacing* ratio in the relay ramp (Soliva and Benedicto, 2004; Imber et al., 2004). Anomalous displacement geometry of a segmented fault has been

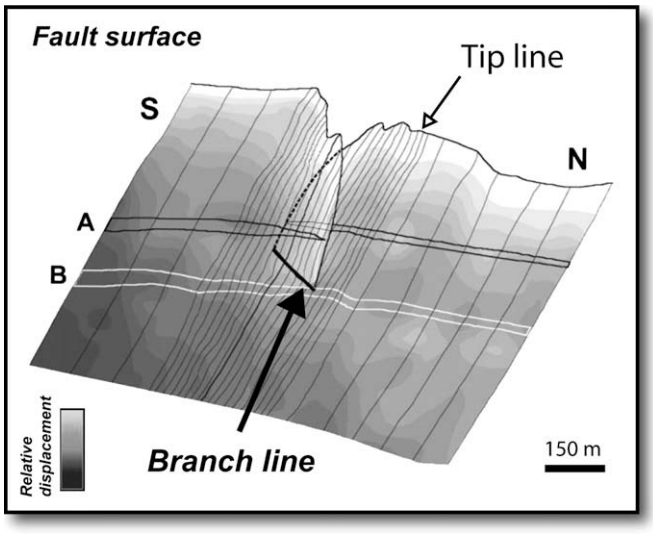


**Fig. 2.** Example of a 3-D fault surface geometry reconstructed from high-resolution 3-D seismic surveys. The fault surface shows two fault segments branched down-dip. The zone of fault segment merging defines a branch line. N and S indicate North and South, respectively, and lines A (black) and B (white) indicate intersections of two different bed horizons with the fault surface. The horizon A shows a segmented fault trace with a relay zone and horizon B shows the continuous fault surface under the branch line. Fine dip parallel lines show positions of cross-sectional interpretations (spaced at 12.5 m in the relay and 62.5 m outside). Note the heterogeneity of the displacement pattern at the relay zone around the branch line (gray scale contours on the fault surface showing relatively large values at left and low at right). After Walsh et al. (2003a,b).

documented by Childs et al. (1995) as "coherent" with the typical profiles of isolated faults, implying an asymmetry of displacement gradient between the interacting segments, i.e. the fault zone exhibits large scatter in displacement–length ($D_{max}/L$) ratio between each segments. A "coherent" displacement profile, as well as the absence of displacement rate increase (see Cowie and Roberts, 2001) during the interaction of unlinked segments seems to be specific to down-dip branched segments (Walsh et al., 2003a,b). The question of the origin of such displacement gradients and low fault segment interaction was not addressed in the previous studies and is the main focus of this paper.

We first present field data from segmented normal faults having particular fault geometries that may be due to down-dip branching of the fault segments at depth. Secondly, we provide a 3-D numerical modeling study of computed displacements and quasi-static stress fields around different geometries of down-dip branched normal fault segments. The results are compared and discussed with respect to the field observations. We apply our study by modeling the Vallo di Diano segmented normal fault (Italy) in order to explain the unexpected displacement profile and low interaction of the largely overlapping segments there. We then discuss the implications of our results for the estimation of maximum earthquake rupture size that could occur on a segmented normal fault.

## 2. Geometrical attributes of down-dip branched normal fault segments

In this section we present field data from two outcrops, the Nigüelas and Fumanyá fault sets, that contain both types of normal fault segmentation, i.e. fault segments separated and down-dip branched segments (Fig. 3). At Nigüelas, the faults cut homogeneous meta-limestone microbreccias, whereas at Fumanyá, the faults are restricted to brittle limestone layers bounded by shales. We refer to Soliva (2004) and Soliva and Benedicto (2004) for details and discussion on the formation and geological context of these fault sets. Down-dip branching is recognized at Nigüelas whereas it is less clear in the layered sequences from Fumanyá (see Fig. 3), since the fault segments there are confined within brittle layers (Soliva et al., 2006).

Displacements at the observation surface were measured along segmented faults containing unlinked relays in the two study areas (Soliva and Benedicto, 2004). All the segment arrays with more than two segments were excluded to avoid the contributions of multiple relay zones to the displacement profiles. The examples of displacement profiles presented in Fig. 4a and b show that unlinked fault segment arrays from Nigüelas have a larger asymmetry in their displacement profiles than comparable structures at Fumanyá. This asymmetry is expressed in the shapes of the profiles and especially in the displacement gradients $G$ adjacent to the relay zones ($G$ defined as $D_{max}$ normalized to the distance between $D_{max}$ and the fault segment tip of the relay zone). In both examples shown in Fig. 4a and b, we can define two values of $G$ ($G_{max}$ and $G_{min}$) corresponding to the two segment ends of the relay zone. Note that the $D_{max}/L$ ratios of the two segments capture part of the displacement asymmetry. The interesting feature to notice is that only the segmented faults from Nigüelas show a large $G_{max}/G_{min}$ ratio (see the three squares indicated with an arrow in Fig. 4c). This seems to occur for fault segment arrays having an especially large overlap/spacing ratio ($O_v/S$). Fig. 4 reveals that both fault displacement and relay zone geometry are characteristic of these three segmented faults from Nigüelas, raising the question, are the displacement distribution and the geometrical attributes of the fault array mechanically related to fault segments branched at depth? In the next section, a numerical modeling analysis is addressed to study the role of different down-dip branching

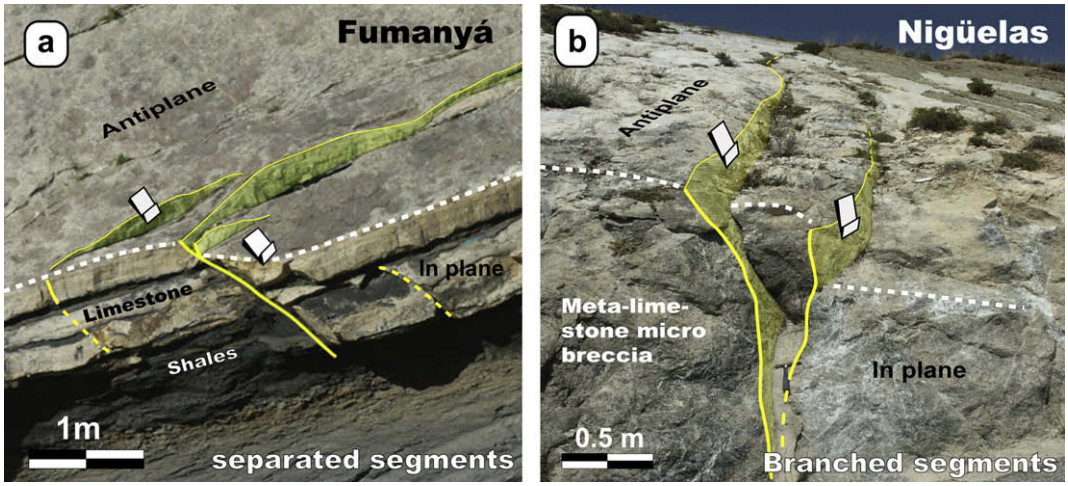


**Fig. 3.** Field examples of (a) separated (Fumanyá) and (b) down-dip branched (Nigüelas) fault segments in homogeneous and layered rocks, respectively. The faults are observed both in anti-plane (normal to shearing) and in-plane (parallel to shearing) dimensions.

geometries on fault displacement distribution and segment interaction.

## 3. Insight from 3-D numerical modeling

In this section we examine the effect of the geometry of fault segment branching at depth on the displacement and stress interaction of the fault segment surfaces. This modeling is performed using Poly3D, a three-dimensional boundary element computer program based on linear elasticity (Jaeger and Cook, 1979) and triangular displacement discontinuity patches (Thomas, 1993). This numerical code has been used to model 3-D quasi-static displacement and stress distributions around simple or complex fault geometries (e.g. Willemse, 1997; Crider and Pollard, 1998; Maerten et al., 1999; Kattenhorn and Pollard, 2001; Soliva et al., 2006).

### 3.1. Three-dimensional branching model geometry

We model the displacement distribution and the quasi-static stress field around three types of normal fault branching geometries defined by two upper segments merging at depth into a single lower fault surface (Fig. 5a). We use three discontinuity surfaces (denoted 1, 2, and 3) in Fig. 5a with an average dip of 60° to build this fault geometry. The discontinuity surfaces 1 and 2 are of $L = 5.5$ m length, $H = 5$ m down-dip height, and surface 3 has 10 m length and 5 m down-dip height. The resulting relay zone has an overlap $O_v$ of 1 m and a spacing of 0.5 m in the horizontal plane (Fig. 5c). The fault geometry has a "branch line" configuration (Fig. 5a) (see the discussion of branch lines and branch points in Childs et al., 1995), which has been inferred from seismic data and field observations (Figs. 2 and 3b).

Around the branch lines we explore variations in the dip of the upper fault segments following three configurations (Fig. 5b). In the first fault configuration the upper frontal segment (2 in Fig. 5a) is coplanar and continuous with the lower fault plane (3), whereas the rear upper segment (1) has a zone of lower dip than the whole fault surface. This gives a sigmoidal geometry with a horizontal corrugation axis along the branch line on the upper horizontal tip of the lower surface (denoted as 3). This results in an asymmetric configuration of a 3-D relay zone branched at depth called here the "*planar frontal segment*".

The second configuration called "*nearly symmetric branching*" is defined by two opposite dip variations, with the same wavelength of sinuosity than the previous configuration and the same dimension of spacing and overlap at the relay zone. The third configuration has the rear upper segment (denoted as 1) coplanar and in continuity with the lower fault plane (denoted as 3), whereas the frontal upper segment (denoted as 2) has a zone of higher dip than the whole fault surface. This gives a sigmoidal geometry of the frontal segment along the branch line on the upper horizontal tip of the lower surface (denoted as 3). We call this configuration the "*planar rear segment*".

### 3.2. Boundary conditions

The boundary conditions applied to the modeled fault are (1) no displacement normal to each polygonal element (only slipping surfaces), (2) triaxial compressive remote stresses, and (3) an elastic full space in order to simulate deep confined faults. We do not apply any shear strength profiles within the faults to reproduce fault end tapering, which primarily affects displacements and the stress concentration near the fault tip. Our results must therefore be considered as the end-member case of maximum elastic–static fault displacement and interaction.

The material properties used are defined by a Poisson's ratio $\nu = 0.25$, a shear modulus of 10 GPa and a density of the overburden $\rho = 2000\ \mathrm{kg.m^{-3}}$. These values are consistent with common values for sedimentary rocks (Hatheway and Kiersch, 1989). The faults are subjected to a lithostatic load, such that $\sigma_V = \rho g z$, where $g$ is the gravitational acceleration and $z$ is the depth within the Earth. The lithostatic load gradient is neglected because of the small down-dip fault dimension ($H = 10$ m), which also justifies the use of homogenous elastic full space rather than an elastic half-space. A horizontal compressive confining stress reduced by a tectonic constant, is also applied. The confining pressure is resolved following a plane-strain configuration in which $\sigma_H = [\nu/(1-\nu)]\sigma_V$ (Jaeger and Cook, 1979, p. 113). The horizontal constant tectonic tension ($T < 0$), is added perpendicular to fault strike, in order to simulate a less compressive stress ($\sigma_h = \sigma_H + T$). These conditions lead to a stress system remotely applied such that $\sigma_1 = \sigma_V$, $\sigma_2 = \sigma_H$ and $\sigma_3 = \sigma_h$. The ratio $\sigma_2/\sigma_3$ has been frequently estimated between 1 and 5 in the sedimentary cover in extensional tectonic settings (Zoback et al., 2003; Christiansson and Janson, 2003). Here we choose a value $\sigma_2/\sigma_3 = 2$. Modeling the half-space problem reveals that 10 m height faults are influenced by the free surface only in the first 100 m depth, so we choose a fault depth of 1 km in order to analyze only the effect of the geometry of fault segment branching on the distribution of displacement and stresses at the overlap zone. This results in the

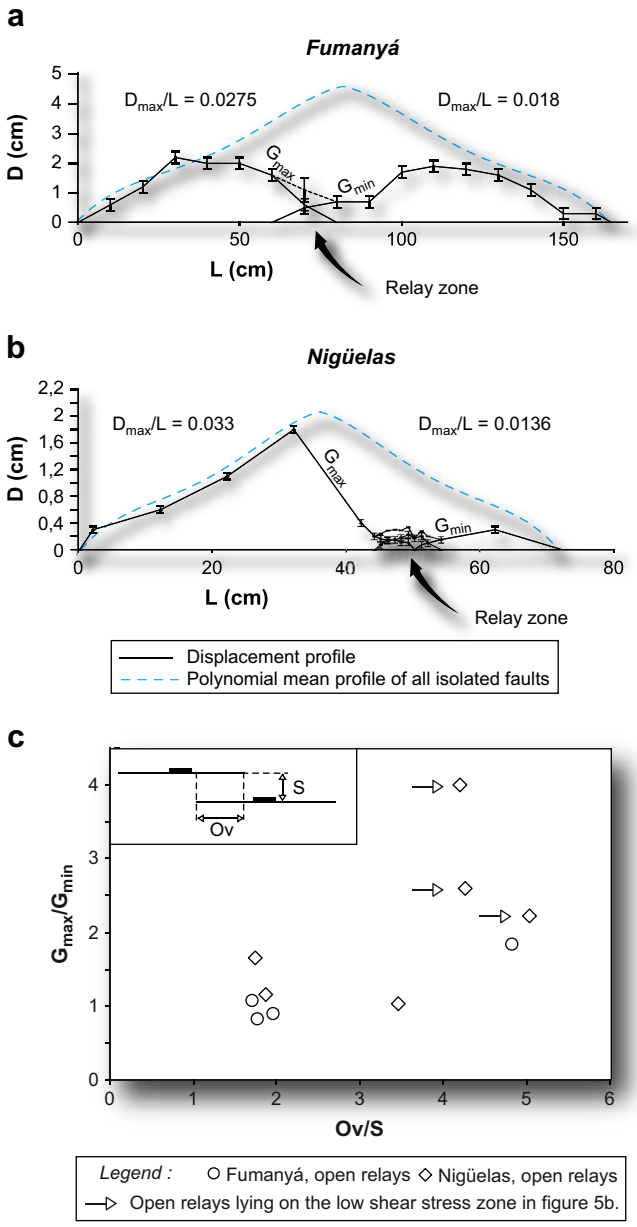


**Fig. 4.** Displacement profiles, displacement gradients ($G_{max}$ and $G_{min}$), and $D_{max}/L$ ratios of unlinked segmented faults showing (a) symmetric displacement profiles at Fumanyá and (b) asymmetric displacement gradients at Nigüelas coherent with isolated fault average profile. (c) Displacement gradient ratios ($G_{max}/G_{min}$) vs. relay aspect ratios ($O_v/S$) from both studied fault systems. Note the occurrence of large $O_v/S$ and $G_{max}/G_{min}$ for three segmented faults at Nigüelas.

following stress magnitudes: $\sigma_1 = 19.6$ MPa, $\sigma_2 = 6.53$ MPa, $\sigma_2 = 3.26$ MPa.

### 3.3. Output conditions

Fault displacement distributions are calculated using Poly3D (Thomas, 1993). The software's graphical interface allows visualization of the displacement distribution along complex 3-D fault surfaces (Figs. 5 and 6).

To analyze fault segment interaction through their stress fields, we calculate the maximum Coulomb shear stress ($S_C$). The maximum Coulomb shear stress is described in linear elasticity theory as a criterion for shear failure (Jaeger and Cook, 1979, p. 95; Crider and Pollard, 1998; Soliva et al., 2006). In our models, $S_C$ has been calculated in the volume of rock surrounding the faults. The maximum Coulomb shear stress is defined as:

$$S_C = \left[\frac{(\sigma_1 - \sigma_3)}{2}\right] \cdot \left(\sqrt{1+\mu^2} - \mu\right) \cdot \left[\frac{(\sigma_1 + \sigma_3)}{2}\right] \quad (1)$$

where $\mu$ is the coefficient of internal friction ($\mu = 0.6$). We analyze the distribution of $S_C$ on horizontal observation grids, crossing the 3-D relay zone through their centers (Fig. 5a and c). In order to compare the results of each model configuration, we present the local values of $S_C$ normalized by the remote value of $S_C$, which is the same for each model (i.e. same boundary conditions, see Section 3.2).

The shear stress perturbation around faults has been used as a criterion for fault interaction through the stress field, new fault initiation around faults, or fault propagation (Ackermann and Schlische, 1997; Willemse, 1997; Crider and Pollard, 1998; Gupta and Scholz, 2000; Maerten et al., 2000; Soliva et al., 2006). This is based on the premise that a fault can initiate or propagate when perturbed $S_C$ (i.e. the local value of $S_C$ in the rock volume near a fault) reaches the inherent shear strength of the material (Jaeger and Cook, 1979, p. 96). The maximum Coulomb shear stress is presented on a horizontal observation grid located at the midpoint depth of the fault surface overlap zone.

### 3.4. Results: displacement patterns and segment interaction

Displacement patterns of the three fault branching configurations (Fig. 5b) are presented by contours of normalized displacement in Fig. 6 on the left side of each figure part. The loss of continuity of the contour curves along the branch line is due to the resolution of the mesh which does not allow imaging the very high displacement gradient around the branch zone (Childs et al., 1995; Walsh et al., 2003a). The resolution is, however, relevant to the whole size of the fault and to the accuracy required to image displacement variations along the upper fault segments due to fault branching. For both the three fault configurations, $D_{max}$ is systematically located on the lower fault plane.

The numerical modeling reveals variations in the displacement pattern on the fault surface. In the *planar frontal segment* configuration (Fig. 6a, left side), the displacement distribution is slightly asymmetric between the frontal and the rear upper segments. The normalized displacement is a little higher on fault segment 1 than on fault segment 2. This is particularly well expressed by a larger extent of the lobe of maximum displacement at the base of fault segment 1 compared to segment 2. For the other configurations, the asymmetry of displacement distribution is much more pronounced, especially in the *planar rear segment* case (Fig. 6c). Here, the displacement distribution on fault segment 1 is a slightly smaller than in the *planar frontal segment* (Fig. 6a) and in the *nearly symmetric branching* (Fig. 6b). In contrast, a reduction of displacement is clearly expressed on fault segment 2: ~15% for the *nearly symmetric branching* configuration and ~25% for the *planar rear segment* configuration. This last case of fault configuration (*planar rear segment*) most contrasts with the case of separated fault segment interaction producing comparable displacement gradients and $D_{max}/L$ ratio along both segments (see Fig. 7 and also see Bürgmann et al., 1994; Willemse et al., 1996; Crider and Pollard, 1998; Martel, 1999).

The normalized shear stress distribution at the relay zone is presented on the horizontal observation grid for each fault model configuration (Fig. 6, right side). A clear increase of normalized $S_C$ within the area of fault segment overlap (and a drop outside) is observed for each fault branching configuration. The maximum value is unambiguously located within the overlap zone near the fault tips, and the value at the center of the overlap zone is slightly different for each fault branching configuration (factors of remote

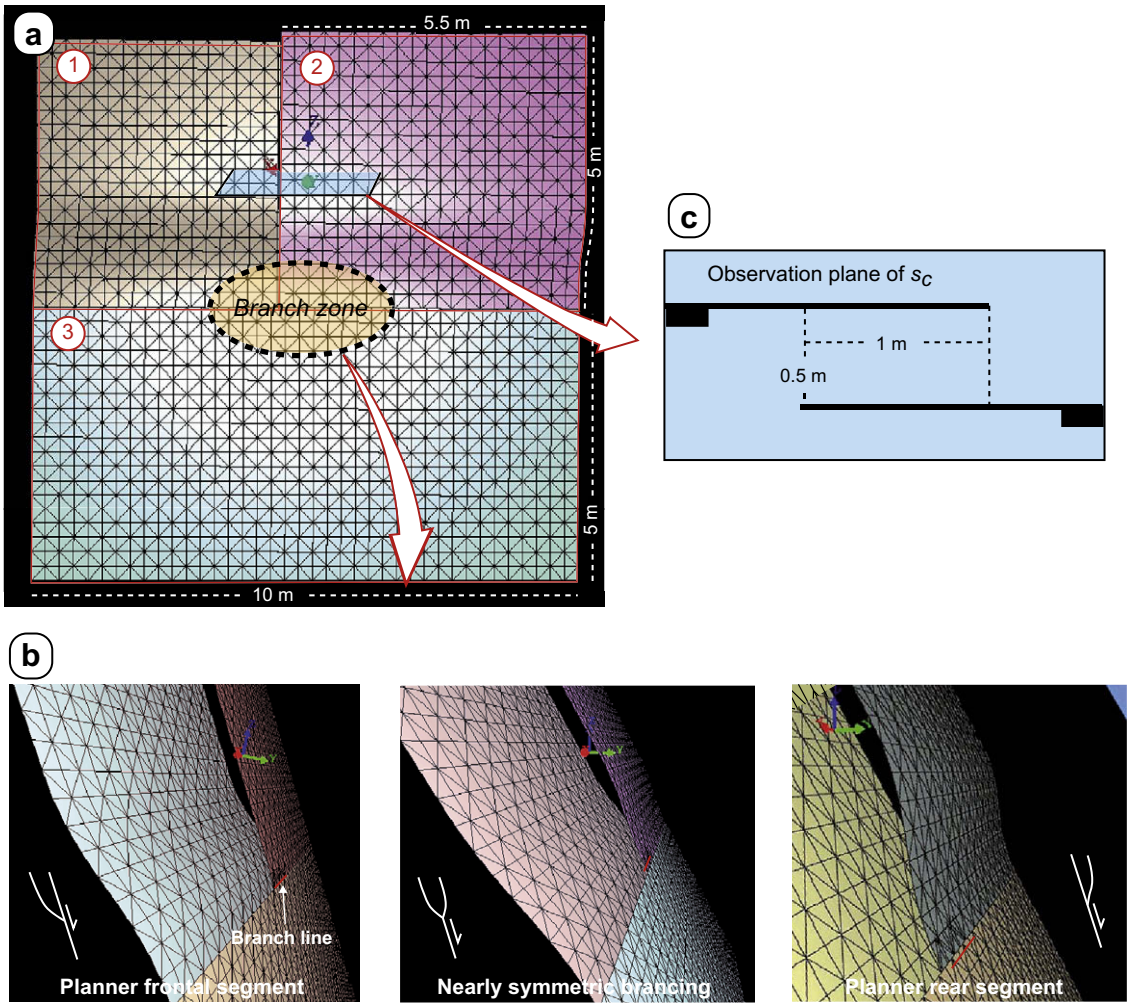


**Fig. 5.** Overview of the 3-D geometry of the segmented faults used in the models. (a) Global view of the 3-D fault mesh and the position of the relay zone observation plane. Three parts of the fault surface are distinguished: (1) the rear segment, (2) the frontal segment and (3) the lower fault surface. (b) 3-D perspective views of the fault branching configuration used in the models. (c) Map view of the observation plane and dimensions of the relay zone.

$S_C$ of 1.404, 1.335 and 1.237 for Fig. 6a, b and c, respectively). The orientation of the principal stress axes $\sigma_2$ and $\sigma_3$ projected on the observation grid remains unchanged on the three models. The projection of the $\sigma_2$ axis is normal to the faults at the center of the overlap and reorients progressively near the fault tips to trend close to the fault strike, but still with a small angle (2°) at the fault tips. The projection of the $\sigma_3$ axis is ~20° oblique at the center of the overlap zone and reorients progressively near the fault tips to trend close to normal to the fault strike, but still with a small obliquity of ~5° at the fault tips. In the *planar frontal segment* fault configuration (Fig. 6a), a lobe of high shear stress increase (factor of remote $S_C > 1.4$, in green) promotes linkage of the fault tips in the center of the overlap zone. In the *nearly symmetric branching* configuration, two lobes of high shear stress are separated and located within the overlap zone close to the fault tips. In the *planar rear segment* configuration, two lobes are also separated and the lobe adjacent to the frontal fault segment (2) is very small and close to the fault tip.

On the horizontal observation grid, quasi-static elastic stress interaction is substantially higher in the case of *planar frontal segment* than for the *nearly symmetric branching* and *planar rear segment* configurations. In other words, fault segment linkage is not favored when high displacement gradient asymmetry is observed (i.e. in the *planar rear segment* model). The trend of a new linking fault that could initiate at the center of the relay zone is approximated by the projection of $\sigma_2$ on the horizontal observation grid (error of ±10°, since the dip of the plane containing $\sigma_2$ and $\sigma_3$ is ≤30°). This trend does not significantly vary with fault branching geometry.

### 3.5. Origin of displacement asymmetry and variable stress interactions

The variation of branching geometry implies changes in quasi-static displacement and stress state on the upper fault segment branches. More precisely, these displacements and stress changes are closely related to the variation of surface dip required for fault branching. The three configurations of fault branching show that fault segment 1 (left side) accommodates higher displacement than segment 2. This is due to more favorable orientation of the fault segment 1 in response to the applied load. When the segment 2 is close to vertical (85° in the *planar rear segment* case) and therefore close to the dip of the $\sigma_1$ axis, it contains a low resolved shear stress that inhibits fault displacement. In contrast, where segment 1 has a 45° dip (see the *planar frontal segment*), the maximum resolved shear stress occurs on this fault portion and enhances fault displacement. The proximity of the fault tip above the branch zone inhibits fault displacement and this effect is similar on both upper fault segment branches.

In the case where the amount of fault displacement is reduced, i.e. the *planar rear segment* case, the displacement gradient near the

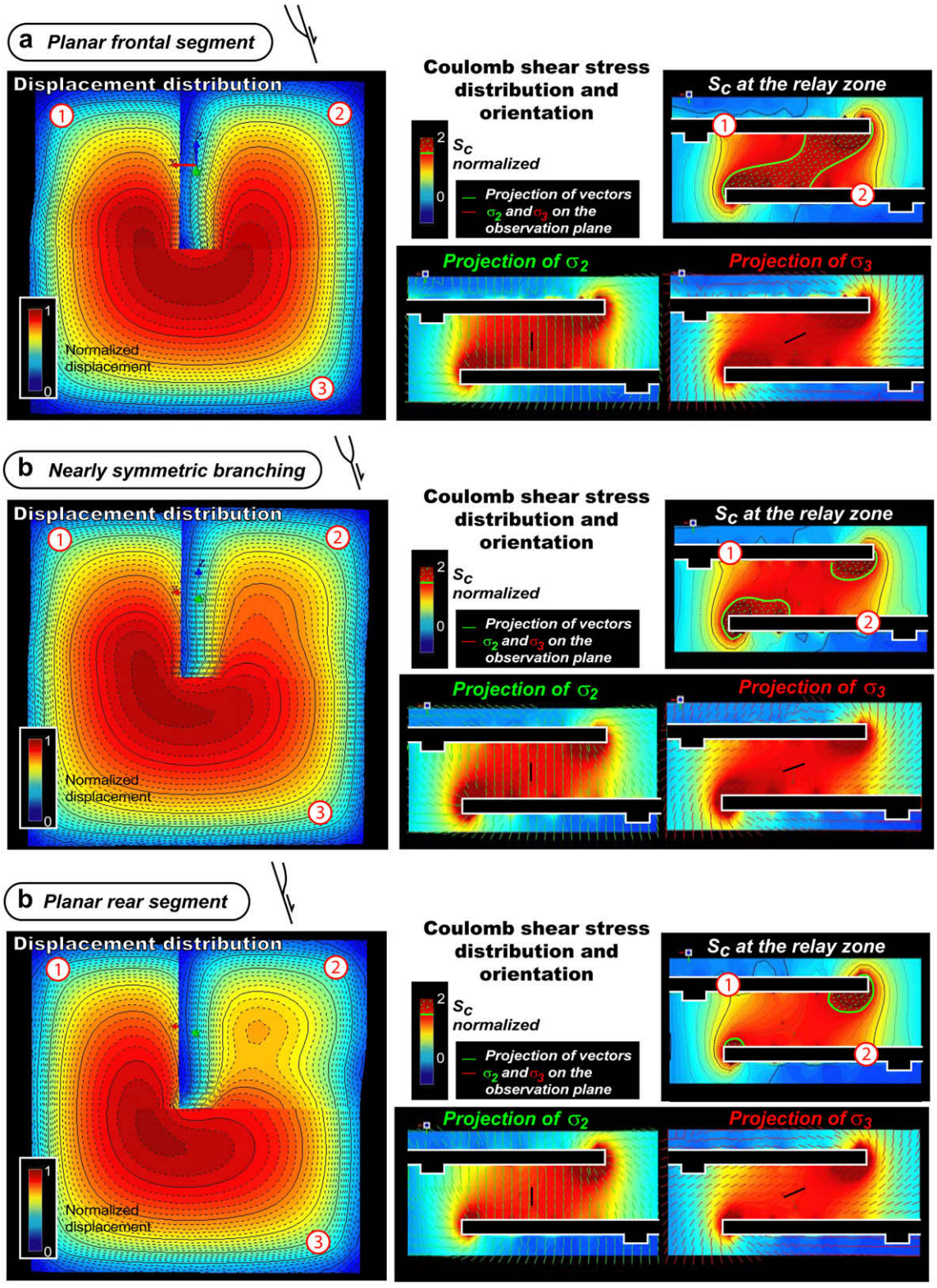


**Fig. 6.** Displacement distribution and stress perturbation on modeled fault surface and on the observation plane at the relay zone (see Fig. 5a), respectively. (a) Results of the "planar frontal segment" fault configuration. Iso-contours of displacement and stresses are shown. Tick marks on relay zone observation planes show the orientation of $\sigma_2$ and $\sigma_3$. (b) Results of the "symmetric branching" fault configuration. (c) Results of the "planar rear segment" fault configuration.

relay zone is consequently reduced. This effect is consistent with the reduced amount of shear stress within the relay zone that is dependent on displacement gradient (Rudnicki, 1977; Cowie and Scholz, 1992; Willemse, 1997; Schultz and Fossen, 2002). On the other hand, where fault displacement is enhanced, i.e. the *planar frontal segment* case, the displacement gradient is larger and stress magnitudes within the relay zone are augmented. Fault interaction and linkage are therefore closely related to fault displacement

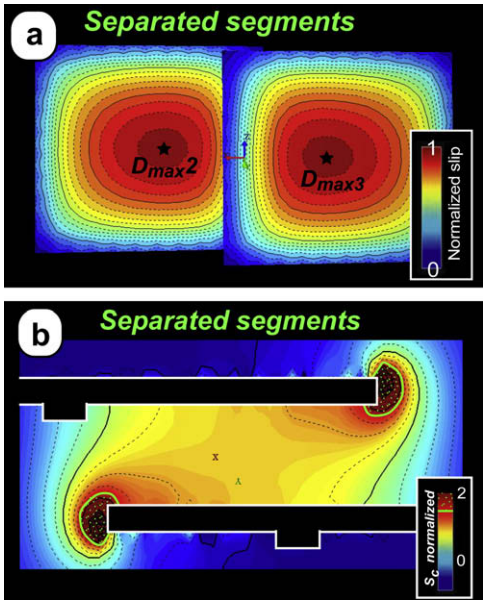


**Fig. 7.** Displacement distribution (a) and relay zone Coulomb shear stress perturbation (b) of separated normal fault segments. The segments have the same dimensions and the same relay zone aspect ratio than the upper segments of Fig. 5 and a dip of 60°. Note the symmetry in the displacement pattern about the overlap zone, leading to anti-symmetry in the horizontal stress distribution at the relay zone. The low amount of displacement on the fault surface (~0.7 $D_{max}$ of Fig. 7a at the center of the upper segment labeled 1) leads to the low accumulation of shear stress in the relay zone compared to the branched segments of Fig. 6.

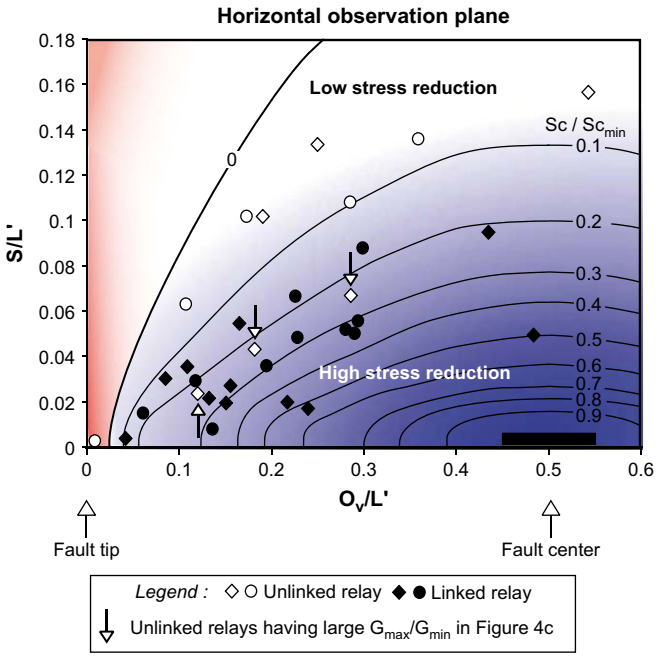


**Fig. 8.** Spacing/segment length ($S/L'$) vs. overlap/segment length ($O_v/L'$) of unlinked and linked fault segments from Fumanyá and Nigüelas. Also shown are contours of $S_C$ computed for an isolated normal fault having a linear displacement distribution from $D_{max}$ to the fault tip. Note the anomalous position of the three unlinked relays from Fig. 4b, lying within the stress drop zone produced by the adjacent fault segment. See text for further explanation.

gradient (see also Soliva and Benedicto, 2004), which is affected by the geometry of fault segment branching at depth.

### 3.6. Discussion on fault interaction from field data and numerical modeling

These variations in fault displacement gradient and fault interaction are consistent with the geometrical attributes of segmented faults observed in the field (Section 2). To quantitatively estimate fault interaction from field data, we have reported in Fig. 8 the data presented in Fig. 4c, shown with linked relay zones. This graphical representation suggested by Gupta and Scholz (2000) has been proposed to estimate the degree of fault interaction. The position of the fault segment tips at the relay zone is reported on a spacing vs. overlap graph in which both parameters are normalized by the length of the adjacent fault segment. On this graph is also reported the Coulomb shear stress perturbation due to displacement on the adjacent fault segment, which has been calculated with the typical nearly linear displacement distribution (polynomial mean) of the studied faults (e.g. Gupta and Scholz, 2000; Soliva and Benedicto, 2004). This approach therefore considers a first-order approximation of fault interaction based on shear stress changes induced on a locked fault by slip on a nearby fault (Gupta and Scholz, 2000). The segmented faults from Nigüelas that have large $G_{max}/G_{min}$ and $O_v/S$ ratios on Fig. 4c are indicated in Fig. 8 with an arrow. These overlapping segments lie anomalously in an area of stress drop (here the stress field produced by only one fault) which should have promoted linkage of the fault segments (Gupta and Scholz, 2000; Soliva et al., 2006). Instead, the faults seem to interact modestly, allowing preservation of their unlinked geometries, even for large values of overlap relative to the fault spacing. We therefore conclude that anomalously large $O_v/S$ ratio along with fault displacement gradient asymmetry (large $G_{max}/G_{min}$ ratio, Fig. 4) reveals low fault segment interaction, as it is observed for *planar rear segment* of Fig. 6c, where the displacement gradients are asymmetric and the shear stress resulting from the interaction of the two fault segment is insufficient to promote fault linkage.

Since fault branching at depth is observed on cross sections at Nigüelas (see Fig. 3a), a source of the displacement asymmetry observed on the data of Fig. 4 is probably due to the presence of fault branching at depth. However, although some faults are observed in section as branched at depth along this outcrop, the 3-D geometry of these segmented faults is not well exposed. In order to provide more constraints on the effect of fault branching, we present in the next section the case study of the Vallo di Diano normal fault zone on which area the seismic history reveals that the overlapping fault segments observed at the surface form a single fault plane at depth.

## 4. Application to a natural case: the Vallo di Diano segmented normal fault

### 4.1. Geological setting

The seismogenic normal fault zone studied in this section is located in the axial zone of the South Apennine belt of Italy. The segmented Vallo di Diano normal fault cuts thrusting sequences of Triassic to Paleogene carbonates overlying Neogene series (e.g. Scandone, 1972; Cello et al., 1989). The segmented normal fault is NW–SE trending and bounds a continental basin (Fig. 9) in-filled during the Pleistocene–Holocene by fluvio-lacustrine sediments. The Monti della Maddalena and the Monti di Sito mountain ridges bound the Vallo di Diano fault zone at the southeast. These mountains contain thrusting units of Mesozoic to Paleogene platform carbonates overlying the Lagonegro basin units (Scandone and Bonardi, 1968). In the northwest, the fault zone affects the Cretaceous to Paleogene series of the Monti Alburni (d'Argenio et al., 1973).

The fault zone, formed later than the Apennines thrust belt, is composed of normal fault segments observed as recent fault scarps

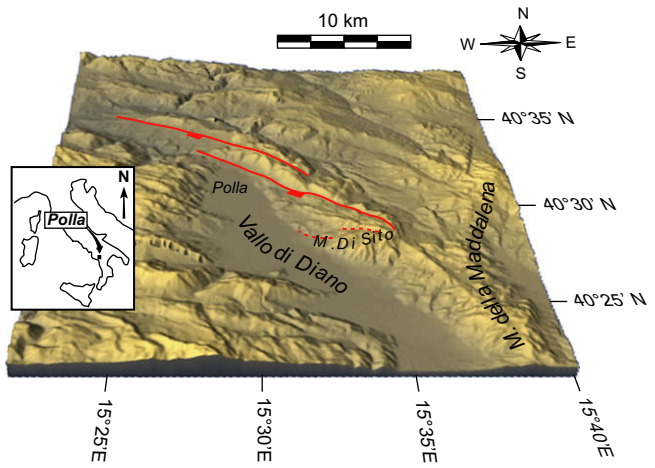


**Fig. 9.** Location and overview of the Vallo di Diano segmented normal fault zone on a digital elevation model (SRTM). The overlapping normal fault segments are mapped with red lines at the base of the fault scarps.

containing triangular facets (Fig. 9). The fault zone is mainly composed of two seismically active fault segments of 14.3 and 15.5 km length, overlapping for a distance along fault strike of 7 km and spaced ~2 km apart (Fig. 10a). The fault planes, frequently outcropping along these two fault segments, show high-angle raking striations indicating a major component of normal displacement, consistent with a subhorizontal least compressive principal stress ($\sigma_3$) oriented N020 (see Cello et al., 2003).

The Vallo di Diano fault produced an earthquake of magnitude 6.4 in 1561, called the Polla earthquake (Boschi et al., 1997). This relatively large magnitude compared to the surface length of the main fault segments (~15 km each) implies the presence of a single continuous rupture surface at depth of about 25 km length, corresponding to the entire length of the segmented fault observed at the surface. To produce an earthquake of magnitude 6.4, Cello et al. (2003) inferred that the fault segments observed as separated at the surface are branched at depth to form a single fault surface allowing a continuous rupture of ~25 km length (also see Spina et al., 2008). This hypothesis is tested below by numerical modeling and analysis of the fault zone geometry.

### 4.2. 3-D model setup and boundary conditions

To set up the fault surface of the model we use the morphology of the mapped fault scarp trace as observed in the field (Fig. 10a). In order to build a simple branch zone of the two fault segments at depth, we use the median trace of the faults at the overlapping zone, which constitutes a reasonable approximation of the Vallo di Diano fault surface trace (Fig. 10a). Since there is no further information on the 3-D geometry of the fault plane, we decide to project at depth the surface trace of the faults. Different decollement levels have been described within the carbonate sediment cover of the area. The main mechanically weak level identified in the sequences has been described as ~700 m thick breccias located between 4 and 5 km depth (Monaco et al., 1998; Pescatore et al., 1999; Lentini et al., 2002). Accordingly, we make the assumption that the rear fault segment becomes nearly flat within the breccia unit and branches into the frontal segment at this depth. We therefore introduce two curvatures of the rear segment to reproduce a low dipping fault plane section and fault branching with the frontal segment to form a single continuous fault plane at depth (Fig. 10b, lateral view). This sigmoidal part of the rear segment is located between 4 and 5 km depth and merges into the branch line at 5 km depth. The seismogenic crustal thickness in this region is at ~15 km depth (Gasparini et al., 1985) and the faults outcrop with an average dip of 65° (Cello et al., 2003). We therefore chose a cross-sectional fault dimension of $H = 16.55$ km. In the model the fault segment lengths simulate surface observations, $L = 14.3$ km and $L' = 15.5$ km, and the total length of the whole fault zone is $L_{tot} = 22.79$ km with an overlap of $O_v = 7$ km and a spacing of $S = 2$ km.

The density of the elastic medium is chosen at 2.5, the Poisson's ratio is $\nu = 0.25$ and the shear modulus is $G = 10$ MPa, which are typical values for rocks of the seismogenic crust (e.g. Hatheway and Kiersch, 1989). The model assumes half-space conditions to simulate the stress-free surface of the Earth. The remote principal stresses applied for a depth of 7.5 km (fault center) are as follows:

$$\sigma_1 = \rho g h = 183.93 \text{ MPa}$$
$$\sigma_2 = [\nu/(1-\nu)]\sigma_1 = 61.31 \text{ MPa}$$
$$\sigma_3 = \sigma_2/3 = 20.43 \text{ MPa}$$

We chose a ratio of $\sigma_2/\sigma_3 = 3$ for this model, which is a reasonable value since this ratio is frequently estimated between 1 and 5 in the sedimentary cover in many tectonic contexts (e.g. Zoback et al., 2003; Martin and Lanyon, 2003; Christiansson and Janson, 2003). The gravitational force is applied following a lithostatic gradient (Anderson, 1951) using $g = 9.81$ m s$^{-2}$ and $\rho = 2500$ kg m$^{-3}$. As in Section 3, we will only analyze the normalized values of the modeled deformations and stresses.

### 4.3. Displacement distribution

Fig. 10b shows different views of the fault zone modeled with contour mapping of the displacement distribution. The fault surface exhibits three lobes of maximum displacement. The first one is located at the Earth's surface on the frontal segment. The second one is located at the center of the fault, underneath the branch line. The third lobe, of lower value, is located at the Earth's surface on the rear segment. Displacement maxima near the Earth's surface are due to the presence of the shear stress-free condition defined by the elastic half-space simulating the Earth surface (also see Nicol et al., 1996; Crider and Pollard, 1998), whereas the maximum displacement at depth is mainly related to the mechanical interaction at the fault branch zone (see also Fig. 6). The main characteristic of the displacement distribution is the asymmetry between the two upper fault segment branches, and particularly at the Earth's surface.

Fig. 10c shows the comparison between the displacement profile measured in the field (Cello et al., 2003) and the displacement profile obtained from numerical modeling. Although the fault segments observed at the surface are of equivalent length, both field data and numerical modeling show an asymmetry in displacement distribution and magnitude around the relay zone. The ratio between displacement maxima is 0.77 for the field data and 0.67 for the numerical model, thus showing a moderate difference of ~10%. This difference, as well as details not reproduced (irregularity in the displacement profile, fault and tapering vs. infinite gradient), is probably due to the assumptions of the simplified numerical model including homogeneous elastic conditions, frictional properties, or details in the fault shape at depth (e.g. Cowie and Scholz, 1992; Willemse, 1997).

The numerical modeling of the displacement pattern shows that the main asymmetry of displacement magnitude between the two fault segments modeled is due to the change of slope of the fault surface at depth, which is required to merge the overlapping fault segments into a single fault plane. More precisely, the low value of displacement observed on the rear segment is due to the low dip zone of the rear upper segment along which

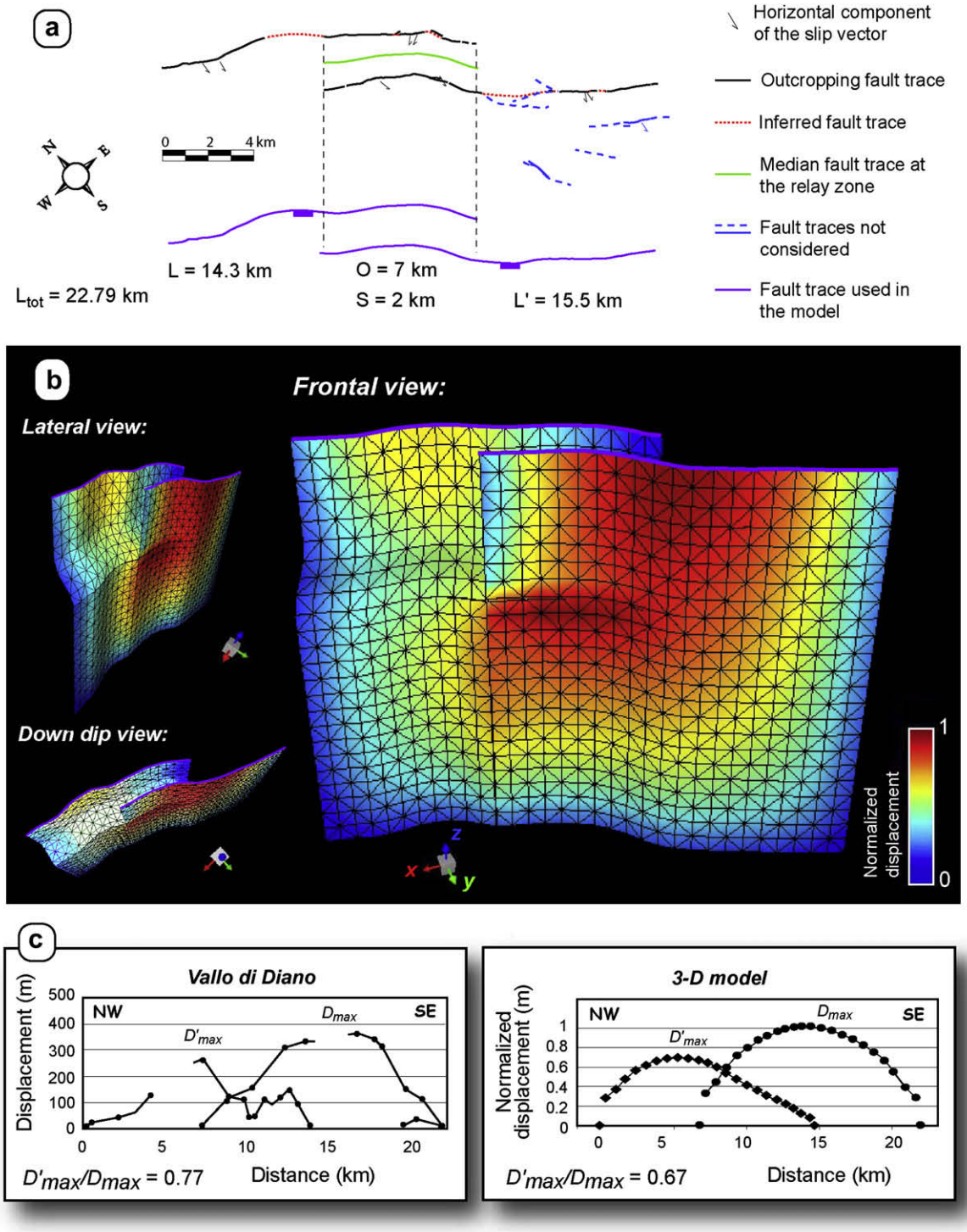


**Fig. 10.** Modeling of the displacement distribution on the Vallo di Diano segmented fault zone. (a) Fault map and surface trace integrated in the model. (b) Three-dimensional views of the fault surface, the mesh used in the model and displacement distribution computed. (c) Comparison between Earth's surface scarp topography profiles and displacement computed at the surface in the model.

fault slip is impeded due to the reduced value of resolved shear stress. This fault zone has an angle of ~60° to the remote orientation of the principal stress axes $\sigma_1$ and therefore has a large component of normal stress acting to resist slip (also see the concept of non-conservative barrier in King and Yielding, 1984). The effect of this fault configuration, not treated in Section 3, constitutes a complementary modeling result demonstrating that displacement asymmetry can be due to locally low normal fault dip.

### 4.4. Fault segment interaction

The stress distribution computed around the fault zone is highly perturbed. Fig. 11a shows the distribution of normalized $S_C$, calculated at the Earth's surface of the fault geometry shown in Fig. 10. This shear stress distribution shows maximum values at the ends of the fault segments, except for the southeastern tip of the rear segment. In contrast with the results shown in Section 3, the overlap zone is not a zone of shear stress increase, but a zone of

stress reduction. The fault morphology used in the model (i.e. the large bend of the rear segment) reduces displacement along the rear segment and therefore implies low interaction of the fault segments which should impede rupture of the relay ramp during an earthquake event. This is consistent with the absence of surface rupture within the overlap zone in the field.

To expand upon this analysis of fault interaction, we compare the geometrical attributes of the fault overlap zone to multiple data sets collected on normal fault relay zones of a broad range scale (see Soliva and Benedicto, 2004 for source data and discussions about the scaling of fault linkage) (Fig. 11b). The parameters measured are *relay displacement* ($D$), the aggregate displacement measured at the fault overlap center, and fault *spacing* ($S$). In contrast to other conventional representations using geometrical attributes of the fault traces at the surface, this graphical representation indirectly considers the influence of fault branching at depth, since it includes the magnitude of displacement which is controlled by the fault geometry at depth. Open relays (modestly interacting unlinked segments), incipiently linked relays (highly interacting) and breached relays (interaction at intersection zone, i.e. physically linked segments) have been differentiated in Fig. 11b. The relay zone of the Vallo di Diano segmented fault fits on the graphical field of open relays, which is consistent with the absence of geomorphologic evidence for fault linkage within the relay ramp. This approach therefore attests to low fault interaction and low probability of fault linkage at the Earth's surface as suggested by the numerical modeling.

Compared to the shear stress distribution resulting from numerical modeling in Section 3 (Fig. 6), the particularly low fault interaction of the Vallo di Diano fault segments is due to the large fault spacing relative to fault displacement (Fig. 11b). As shown in Section 4.3, the low amount of displacement is due to the shallowly dipping part of the rear fault segment, which explains why this overlapping zone is poorly interacting and therefore not linked (compared to frequently linked or at least highly fractured relays in other examples that have a comparable ratio of $O_v/S = 3.5$, see Aydin and Nur, 1982; Peacock and Sanderson, 1991; Willemse et al., 1996; Crider and Pollard, 1998; Accocella et al., 2000; Gupta and Scholz, 2000; Soliva and Benedicto, 2004; Soliva and Schultz, 2008).

## 5. Implication for potential earthquake rupture size

Although a seismic rupture can jump from one segment to another during a single co-seismic event (e.g. the case of Landers, King and Lin, 1992), it has been inferred that large relay zones of segmented faults can constitute barriers to rupture propagation (see for example the North Anatolian Fault rupture sequence, 1912–1999, Stein et al., 1997). This process is well known on normal, strike slip, and thrust fault relays (e.g. Machete et al., 1991; Ward and Goes, 1993; Jackson et al., 1996). Seismic hazard assessment is currently based on probabilistic approaches (e.g. Working Group on California Earthquake Probabilities, 1999). In such probabilistic studies, the geometry of fault segmentation is considered and any information indicating the geometry of fault at depth is important to constrain the probability of earthquake rupture size.

In this paper we have shown that fault branching at depth can promote asymmetry of fault displacement on fault segments and thereby reduce their ability to interact and link laterally. Branching at depth can therefore reduce fault interaction and the fault's ability to link at the surface, thus promoting preservation of the segmentation observed at the Earth's surface. This suggests that even if the segments are branched at depth, fault segmentation may prevail over long timescales at the surface and that such geometries could be a common feature of active branched faults. In active extensional tectonic settings (e.g. Apennines, gulf of Patras–Corinth, Nevada, East African rift), the seismic hazard inferred from surface fault traces may therefore be underestimated.

We propose that in such areas, the fault scarps must be inspected with respect to their displacement profiles and overlap – separation data (see for example Fig. 4) in order to reveal any asymmetry of displacement gradient coupled with a large $O_v/S$ ratio of the fault segments. This will identify which segmented fault could be a good candidate to produce an earthquake size larger than the segmentation length observed, and would accordingly need to be emphasized by seismotectonic analysis.

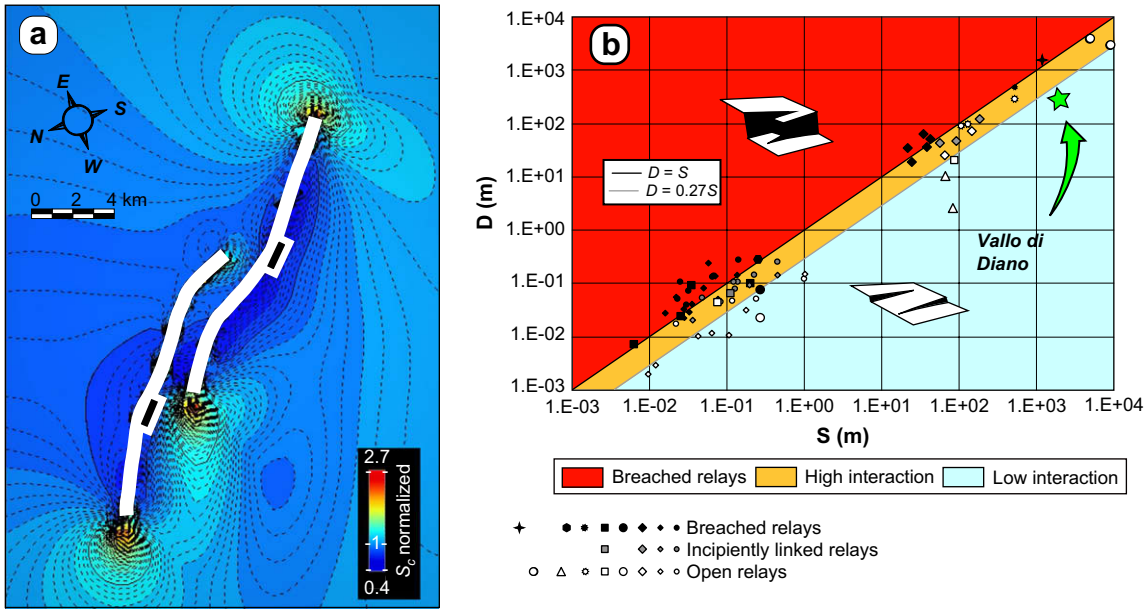


**Fig. 11.** Fault segment interaction at the Earth's surface. (a) Map of normalized $S_C$ computed with the fault geometry shown in Fig. 9. Note the presence of a low shear stress zone at the area of fault segment overlap. (b) Graph of relay displacement ($D$, total displacement measured at the center of the overlap zone) vs. spacing ($S$) of unlinked, incipiently linked and fully breached relay zones, after Soliva and Benedicto (2004). The position of the Vallo di Diano field data on the graph and the low stress accumulation at the relay zone suggest low fault interaction at the Earth's surface.

## 6. Conclusion

The analysis provided in this paper shows that fault segments branched at depth are associated with particular variations in $D_{max}/L$ ratio and displacement gradients close to the relay zones. This effect is principally due to the variation of the fault segment surface dip which is required above the zone where the fault segments branch. In addition,

- Faults segments can have variable $D_{max}/L$ ratios depending on whether they are separate or branched at depth and depending on their particular branching geometry. Fault branching at depth can therefore explain a component of the scatter typically observed on $D_{max}$–$L$ diagrams.
- Faults segments can have variable ability to link at relay zones depending on whether they are separate or branched at depth. This is due to the influence of branching at depth on the shear stress distribution within the relay zone. Fault branching at depth can therefore explain a component of the scatter typically observed on $O_v$–$S$ diagrams.
- Modeling fault segment displacement and interaction of the Vallo di Diano normal fault in Italy suggests that the fault segments are only modestly interacting at the surface although a fault rupture can propagate and break the entire fault length at depth. This shows that little fault segment interaction at the surface can occur on faults branched at depth, and therefore that the fault zone can produce a larger earthquake rupture than what it is expected from the surface length, overlap and spacing of the fault segments.
- We propose that displacement gradient asymmetry and anomalies in overlap-spacing values of the relay zones compared to typical values may be indicators of fault branching at depth. These geometrical attributes of the fault zone should be considered in fault seismotectonic studies in order to estimate the maximum earthquake rupture size along a fault segmented at the surface.

## Acknowledgments

The results presented in this work started during PhD research by the first author at Université Paris XI, Orsay, France and were further developed during work at Université Montpellier II, France. We wish to thank Hervé Philip for useful discussions about seismic hazards. Constructive reviews provided by Michele Cooke and Steven Micklethwaite helped to improve the manuscript. RAS was supported by a grant from NASA's Planetary Geology and Geophysics Program.

## References

Accocella, V., Gudmundsson, A., Funiciello, R., 2000. Interaction and linkage of extension fractures and normal faults: examples from rift zone of Iceland. Journal of Structural Geology 22, 1233–1246.

Ackermann, R.V., Schlische, R.W., 1997. Anticlustering of small normal faults around larger faults. Geology 25, 1127–1130.

Anderson, E.M., 1951. The Dynamics of Faulting. Oliver and Boyd, Edinburgh.

d'Argenio, B., Pescatore, T., Scandone, P., 1973. Schema geologico dell'Appennino meridionale. Atti della Accademia Nazionale dei Lincei 183, 49–72.

Aydin, A., Nur, A., 1982. Evolution of pull-apart basins and their scale independence. Tectonics 1, 91–105.

Benedicto, A., Rives, T., Soliva, R., 2004. The 3D fault segmentation development: a conceptual model. Implications on fault sealing. In: EAGE Conference on Fault and Top Seals: What do We Know and Where do We Go? Extended Abstracts Special Volume. ISBN 90-73781-32-9.

Boschi, E., Guidoboni, E., Ferrari, G., Valensise, G., Gasperini, P., 1997. Catalogo dei forti terremoti in Italia. dal 461 a.C. al 1990, vol. 2. ING-SGA, Bologna.

Boyer, S.E., Elliott, D., 1982. Thrust systems. American Association of Petroleum Geologists Bulletin 66, 1196–1230.

Bürgmann, R., Pollard, D.D., Martel, S.J., 1994. Slip distributions on faults: effects of stress gradients, inelastic deformation, heterogeneous host-rock stiffness, and fault interaction. Journal of Structural Geology 16, 1675–1690.

Cello, G., Tondi, E., Micarelli, L., Mattioni, L., 2003. Active tectonics and earthquake sources in the epicentral area of the 1857 Basilicata earthquake (Southern Italy). Journal of Geodynamics 36, 37–50.

Childs, C., Watterson, J., Walsh, J.J., 1996. A model for the structure and development of fault zones. Journal of the Geological Society of London 153, 337–340.

Cello, G., Martini, N., Paltrinieri, W., Tortorici, L., 1989. Structural styles in the frontal zones of the southern Apennines, Italy: an example from the Molise district. Tectonics 8, 753–768.

Childs, C., Watterson, J., Walsh, J.J., 1995. Fault overlap zones within developing normal fault system. Journal of the Geological Society of London 152, 535–549.

Christiansson, R., Janson, T., 2003. A test of different stress measurement methods in two orthogonal bore holes in Äspö Hard Rock Laboratory (HRL). International Journal of Rock Mechanics and Mining Sciences 40, 1161–1172.

Cowie, P., Roberts, G.P., 2001. Constraining slip rates and spacings for active normal faults. Journal of Structural Geology 23, 1901–1915.

Cowie, P.A., Scholz, C.H., 1992. Physical explanation for the displacement–length relationship of faults using a post-yield fracture mechanics model. Journal of Structural Geology 14, 1133–1148.

Crider, J.G., Pollard, D.D., 1998. Fault linkage: three-dimensional mechanical interaction between echelon normal faults. Journal of Geophysical Research 103, 24373–24391.

Ferrill, D.A., Stamatakos, J.A., Sims, D., 1999. Normal fault corrugation: implications for growth and seismicity of active normal faults. Journal of Structural Geology 21, 1027–1038.

Gasparini, C., Iannaccone, G., Scarpa, R., 1985. Fault-plane solutions and seismicity of the Italian peninsula. Tectonophysics 117, 59–78.

Gupta, A., Scholz, C.H., 2000. A model of normal fault interaction based on observation and theory. Journal of Structural Geology 22, 865–879.

Hatheway, A.W., Kiersch, G.A., 1989. Engineering properties of rock. In: Carmichael, R.S. (Ed.), Practical Handbook of Physical Properties of Rocks and Minerals. CRC Press, Boca Raton, FL, pp. 672–715.

Huggins, P., Watterson, J., Walsh, J.J., Childs, C., 1995. Relay zone geometry and displacement transfer between normal faults recorded in coal-mine plans. Journal of Structural Geology 17, 1741–1755.

Imber, J., Tuckwell, G.W., Childs, C., Walsh, J.J., Manzocchi, T., Heath, A.E., Bonson, C.G., Strand, J., 2004. Three-dimensional distinct element modelling of relay growth and breaching along normal faults. Journal of Structural Geology 26, 1897–1911.

Jackson, J., Norris, A., Youngson, J., 1996. The structural development of active thrust and fold systems in central Otago, New Zealand: evidence revealed by drainage pattern. Journal of Structural Geology 18, 217–234.

Jaeger, J.C., Cook, N.G.W., 1979. Fundamentals of Rock Mechanics. Chapman and Hall, New York, 585 pp.

Kattenhorn, S.A., Pollard, D.D., 2001. Integrating 3D seismic data, field analogs and mechanical models in the analysis of segmented normal faults in the Wytch Farm oil field, southern England. American Association of Petroleum Geologists Bulletin 85, 1183–1210.

King, G.C.P., Lin, J., 1992. Change in failure stress on the southern San Andreas fault system cause by the 1992 magnitude 7.4 Landers earthquake. Science 258, 1328–1332.

King, G.C.P., Yielding, G., 1984. The evolution of a thrust fault system: processes of rupture initiation, propagation and termination in the 1980 El Asnam (Algeria) earthquake. Geophysical Journal of the Royal Astronomical Society 77, 915–933.

Koledoye, A.B., Aydin, A., May, E., 2000. Three dimensional visualization of normal fault segmentation and its implication for fault growth. The Leading Edge 19, 691–701.

Koledoye, A.B., Aydin, A., May, E., 2003. A new process-based methodology for analysis of shale smear along normal faults in the Niger Delta. American Association of Petroleum Geologists Bulletin 87, 445–463.

Lentini, F., Carbone, S., Di Stefano, A., Guarnieri, P., 2002. Stratigraphical and structural constraints in the Lucanian Apennines (southern Italy): tools for reconstructing the geological evolution. Journal of Geodynamics 34, 141–158.

Machete, M.N., Personius, S.F., Nelson, A.R., Schwartz, D.P., Lund, W.R., 1991. The Wasatch fault zone, Utah, segmentation and history of Holocene earthquakes. Journal of Structural Geology 13, 137–149.

Maerten, L., Pollard, D.D., Karpuz, R., 2000. How to constrain 3-D fault continuity and linkage using reflection seismic data: a geomechanical approach. American Association of Petroleum Geologists Bulletin 84, 1311–1324.

Maerten, L., Willemse, E.J.M., Pollard, D.D., Rawnsley, K., 1999. Slip distribution on intersecting normal faults. Journal of Structural Geology 21, 259–271.

Mansfield, C.S., Cartwright, J.A., 1996. High resolution fault displacement mapping from three-dimensional seismic data: evidence for dip linkage during fault growth. Journal of Structural Geology 18, 249–263.

Mansfield, C., Cartwright, J., 2001. Fault growth by linkage: observations and implications from analogue models. Journal of Structural Geology 23, 745–763.

Marchal, D., 1997. Approche spatio-temporelle des mécanismes de la propagation des failles normales: des modélisations analogiques à la sismique 3D. PhD Thesis, Université Henry Poincaré-Nancy I.

Marchal, D., Guiraud, M., Rives, T., 2003. Geometric and morphologic evolution of normal fault planes and traces from 2D to 4D data. Journal of Structural Geology 25, 135–158.

Martel, S.J., 1999. Mechanical controls on fault geometry. Journal of Structural Geology 21, 585–596.

Martin, C.D., Lanyon, G.W., 2003. Measurement of in-situ stress in weak rocks at Mont Teni Rock Laboratory, Switzerland. International Journal of Rock Mechanivs and Mining Sciences 40, 1077–1088.

McGrath, A.G., Davison, I., 1995. Damage zone geometry around fault tips. Journal of Structural Geology 17, 1011–1024.
McLeod, A., Dawers, N.H., Underhill, J.R., 2000. The propagation and linkage of normal faults: insight from the Strathspey–Brent–Statfjord fault array, northern North Sea. Basin Research 12, 263–284.
Monaco, C., Tortorici, L., Paltrinieri, W., 1998. Structural evolution of the Lucanian Apennines. Journal of Structural Geology 20, 617–638.
Nicol, A., Watterson, J., Walsh, J.J., Childs, C., 1996. The shapes, major axis orientations and displacement patterns of fault surfaces. Journal of Structural Geology 18, 235–248.
Peacock, D.C.P., Sanderson, D.J., 1991. Displacement, segment linkage and relay ramps in normal fault zones. Journal of Structural Geology 13, 721–733.
Pescatore, T., Renda, P., Schiattarella, M., Tramutoli, M., 1999. Stratigraphic and structural relationships between Meso-Cenozoic Lagonegro basin and coeval carbonate platforms in southern Apennines, Italy. Tectonophysics 315, 269–286.
Philip, H., Rogozhin, E., Cisternas, A., Bousquet, J.-C., Borisov, B., Karakhanian, A., 1992. The Armenian earthquake of 1988 December 7: faulting and folding, neotectonics and paleaseismicity. Geophysical Journal International 110, 141–158.
Rudnicki, J.W., 1977. The inception of faulting in a rock mass with a weakened zone. Journal of Geophysical Research 82, 844–854.
Scandone, P., 1972. Studi di geologia lucana: carta dei terreni della serie calcareo-silico-marnosa e note illustrative. Bollettino della Societa dei Naturalisti in Napoli 81, 225–300.
Scandone, P., Bonardi, G., 1968. Synsedimentary tectonic controlling of Mesozoic and tertiary carbonate sequence of areas surrounding Vallo di Diano. Memorie della Societa Geologica Italiana 7, 1–10.
Schultz, R.A., Fossen, H., 2002. Displacement–length scaling in three dimensions: the importance of aspect ratio and application to deformation bands. Journal of Structural Geology 24, 1389–1411.
Soliva, R., 2004. Croissance des failles normales dans les séries stratifiées hétérogènes, Rôle de la restriction verticale et de la coalescence sur les lois d'échelles et la distribution spatiale des failles, exemples naturels et approche théorique. PhD Thesis, Université Paris XI.
Soliva, R., Benedicto, A., 2004. A linkage criterion for segmented normal faults. Journal of Structural Geology 12, 2251–2267.
Soliva, R., Benedicto, A., Maerten, L., 2006. Spacing and linkage of confined faults: the importance of mechanical thickness. Journal of Geophysical Research 111, B01402, doi:10.1029/2004JB003507.
Soliva, R., Schultz, R.A., 2008. Distributed and localized faulting in extensional settings: insight from the North Ethiopian Rift–Afar transition area. Tectonics 27, TC2003, doi:10.1029/2007TC002148.
Spina, V., Tondi, E., Galli, P., Mazzoli, S., Cello, G., 2008. Quaternary fault segmentation and interaction in the epicentral area of the 1561 earthquake (Mw = 6.4), Vallo di Diano, southern Apennines, Italy. Tectonophysics 153, 233–245.
Stein, R.S., Barke, A.A., Dieterich, J.H., 1997. Progressive failure on the North Anatolian fault since 1939 by earthquake stress triggering. Geophysical Journal International 128, 594–604.
Thomas, A.L., 1993. Poly3D: a three-dimensional, polygonal element, displacement discontinuity boundary element computer program with applications to fractures, faults, and cavities in the earth's crust. MS Thesis, Stanford University, Stanford, California.
Vermilye, J.M., Scholz, C.H., 1999. Fault propagation and segmentation: insight from the microstructural examination of a small fault. Journal of Structural Geology 21, 1623–1636.
Wallace, R.E., Davis, J.F., McNally, K.C., 1984. Terms for expressing earthquake potential, prediction and probability. Seismological Society of America Bulletin 74, 1819–1825.
Walsh, J.J., Bailey, W.R., Childs, C., Nicol, A., Bonson, C.G., 2003a. Formation of segmented normal faults: a 3-D perspective. Journal of Structural Geology 26, 399–400.
Walsh, J.J., Bailey, W.R., Bonson, C.G., Childs, C., Nicol, A., Schoepfer, M.P., 2003b. How Significant is Segment Linkage in Fault Growth? American Geophysical Union (Fall Meeting 2003, abstract T21B-06).
Walsh, J.J., Watterson, J., Bailey, W.R., Childs, C., 1999. Fault relays, bends and branch-lines. Journal of Structural Geology 21, 1019–1026.
Ward, S.N., Goes, S.D.B., 1993. How regularly do earthquakes recur? A synthetic seismicity model for the San Andreas fault. Geophysical Research Letters 20, 2131–2134.
Willemse, E.J.M., Pollard, D.D., Aydin, A., 1996. Three-dimensional analyses of slip distributions on normal fault arrays with consequences for fault scaling. Journal of Structural Geology 18, 295–309.
Willemse, E.J.M., 1997. Segmented normal faults: correspondence between three-dimensional mechanical models and field data. Journal of Geophysical Research 102, 675–692.
Working Group on California Earthquake Probabilities, 1999. Major quake likely to strike between 2000 and 2030. In: U.S. Geological Survey Fact Sheet, pp. 152–99.
Young, M.J., Gawthorpe, R.L., Hardy, S., 2001. Growth and linkage of a segmented normal fault zone; the late Jurassic Murchinson–Statfjord North Fault, northern North Sea. Journal of Structural Geology 23, 1933–1952.
Zoback, M.D., Barton, C.A., Brudy, M., Castillo, D.A., Finkbeiner, T., Grollimund, B.R., Moos, D.B., Peska, P., Ward, C.D., Wiprut, D.J., 2003. Determination of stress orientation and magnitude in deep wells. International Journal of Rock Mechanics and Mining Sciences 40, 1049–1076.